· Review · Advances in Polar Science
doi: 10.13679/j.advps.2019.1.00011 March 2019 Vol. 30 No. 1: 11-23

Interplanetary shock-associated aurora

LIU Jianjun[1*], HU Hongqiao[1], HAN Desheng[2] & YANG Huigen[1]

[1] SOA Key Laboratory for Polar Science, Polar Research Institute of China, Shanghai 200136, China;
[2] State Key Laboratory of Marine Geology, School of Ocean and Earth Science, Tongji University, Shanghai 20092, China

Received 28 August 2018; accepted 20 December 2018

Abstract Interplanetary shocks or solar wind pressure pulses have prompted impacts on Earth's magnetospheric and ionospheric environment, especially in causing dynamic changes to the bright aurora in the polar ionosphere. The auroral phenomenon associated with shock impingements, referred to as shock aurora, exhibits distinct signatures differing from other geophysical features on the dayside polar ionosphere. Shock aurora provides a direct manifestation of the solar wind–magnetosphere–ionosphere interaction. Imagers onboard satellites can obtain the associated large-scale auroral characteristics during shock impingement on the magnetopause. Therefore, auroral data from satellites are very useful for surveying the comprehensive features of shock aurora and their general evolution. Nonetheless, the ground-based high temporal-spatial resolution all-sky imagers installed at scientific stations play an essential role in revealing medium- and small-scale characteristics of shock aurora. Here, we focus on shock aurora imaging signatures measured by imagers onboard satellites and ground-based all-sky imagers.

Keywords **interplanetary shock, sudden impulse, shock aurora, wave-particle interaction, field-aligned current**

Citation: Liu J J, Hu H Q, Han D S, et al. Interplanetary shock-associated aurora. Adv Polar Sci, 2019, 30(1): 11-23, doi:10.13679/j.advps.2019.1.00011

1 Introduction

It is well known that the interplanetary magnetic field (IMF) accompanying the solar wind exhibits significant control over Earth's magnetospheric configuration and energy transfer. The coupling of the solar wind and the magnetosphere leads to mass, momentum, and energy inputs from interplanetary space into the magnetospheric cavity by the so-called magnetic merging and viscous-like processes mainly occurring in the magnetopause. When the IMF B_z component is southward (specifically negative B_z), the geomagnetic and IMF lines merge near the front of the magnetosphere resulting in the Dungey convection cycle (Dungey, 1961). From ground observations, a viscous-like interaction was proposed whereby the solar wind lost some particles, momentum, and energy in its interaction with the magnetosphere (Axford and Hines, 1961).

However, interplanetary (IP) shocks or solar wind pressure pulses, which are accompanied by a sudden solar wind dynamic pressure enhancement due to changes in either plasma density or velocity, are increasingly found to play an essential role over the size and oval shape of aurora (Chua et al., 2001; Boudouridis et al., 2003; Guo et al., 2005; Liou et al., 2007; Laundal and Østgaard, 2008). Previous work has shown that IP shocks induce a sudden compression of the magnetosphere and greatly disturb Earth's electromagnetic environment. An IP shock frequently induces enhanced dayside auroral emissions and nightside substorm-like activities (Zhou and Tsurutani, 1999, 2001; Zhou et al., 2003, 2009; Motoba et al., 2009; Liu et al., 2011, 2015). Consequently, this influence over the magnetospheric configuration has a corresponding impact on the size and location of the auroral oval and polar cap,

* Corresponding author, E-mail: liujianjun@pric.org.cn

and the associated auroral intensity, cross polar cap potential, field-aligned currents (FACs), and ionospheric convection (Boudouridis et al., 2003, 2007, 2008; Liu et al., 2011; Gao, 2012).

The aurora associated with IP shocks usually presents interesting features that are different from typical auroral activity on the dayside and nightside. Often referred to as "shock aurora", these initially bright transient auroral emissions are usually observed around the magnetic local noon region after the arrival of an IP shock at the dayside magnetopause. As the IP shock propagates past Earth, the shock aurora expands longitudinally to the dawn and dusk sides along the auroral oval flanks with typical ionospheric propagating speeds of 6–11 km·s^{-1}, and eventually reaches the midnight sector after several minutes (Zhou and Tsurutani, 1999; Zhou et al., 2003, 2009; Motoba et al., 2009; Holmes et al., 2014). The shock auroral propagation speed, when mapped from the auroral oval to the magnetospheric equatorial plane, is thought to agree with the speed of the IP shock along the magnetopause (Zhou and Tsurutani, 1999; Zhou et al., 2017). This type of evolution of the shock aurora corresponds to the nominal slower response to the external sudden impingement (Zhou and Tsurutani, 1999). Nevertheless, there are some reports about near-instantaneous (~1–2 min or less) auroral enhancement over a part of or the entire auroral oval just after the shock arrival (Zesta et al., 2000; Chua et al., 2001, Hong et al., 2001; Boudouridis et al., 2003; Meurant et al., 2003). This type of shock aurora appears almost simultaneously (within a few minutes) from noon to the nightside sector.

Comparing our understanding of shock aurora with evidence from global imaging, we have scant knowledge about the forms and intensity of shock aurora occurring during IP shock compression and how its forms and intensifies with time. There is no doubt that ground-based all-sky optical measurements have an ideal advantage in recording shock aurora with high temporal and spatial resolution than any other types of instruments onboard satellites. These ground-based optical measurements do definitely contribute in addressing these questions concerning shock auroral forms; although the ground-based observations often suffer from various interferences such as clouds, moonlight, and sun light.

Here, we give an account of the observational results, including satellite and ground-based measurements, and associated studies on the generation mechanism of shock aurora. In particular, the purpose of this article is to review the development of the fine-scale shock aurora using all-sky optical measurements from ground-based observatories, and to present also some associated studies employing multi-scale auroral imagers and related ionospheric instruments, which in the future will hopefully be announced and investigated through scientific expeditions of the Chinese Arctic and Antarctic Administration.

2 Large-scale features from satellite measurements

IP shocks can greatly disturb Earth's magnetic field, triggering a sudden impulse (SI) or sudden commencement (SC) that manifests as a steplike increase in the northward component of the geomagnetic field observed by low-latitude ground magnetometers (Araki, 1994; Han et al., 2007). As introduced above, just after the SI/SC, transient auroral emissions as observed by satellite develop on a part of the auroral oval on a global scale. As coverage in capturing ultraviolet images is good, satellites have observed quite comprehensively the evolution of the shock aurora over the past three decades (Spann et al., 1998; Tsurutani, 1998, 2001; Zhou and Tsurutani, 1999; Brittnacher et al., 2000; Chua et al., 2001; Hong et al., 2001; Tsurutani et al., 2001, 2011; Zhou et al., 2003; Su et al., 2011).

With data from the large-scale ultraviolet imager (UVI) on NASA's Polar satellite with 3-min cadence, Zhou and Tsurutani (1999) presented two instances of an auroral response to the sudden shock/pressure-wave (Mach number ~2.1) compression within the magnetosphere. By reviewing the sequential response timing to the IP shock in the ionosphere and the global evolution of the dayside auroral phenomenon, Zhou and Tsurutani (1999) found that dayside auroral brightening occurred initially at magnetic local noon region within ~3 min of the shock arrival (roughly marked by the SC/SI onset) and then propagated toward the dawn side and dusk side along the auroral oval. Figure 1 shows the effect of the shock impingement on the auroral oval as seen in the Lyman–Birge–Hopfield (LBH) long filter mode images from the UVI instrument on board the Polar satellite. Shock arrival time is marked by the downward black arrow. The initial response of the auroral oval to the IP shock is found to be in images between 01:00:44 UT and 01:03:48 UT (Figures 1b and 1c). At 01:13:00 UT (Figure 1f), the shock aurora enhancement reaches the nightside sector nearest to midnight. By analyzing this propagation from UVI imagery, they determined that the average ionospheric longitudinal speed of shock aurora was ~6 and ~11 km·s^{-1} in the dusk side and dawn side, respectively, and argued that the auroral brightening and motion are associated with the arrival of shock structure and propagation. With ground-based meridian scanning photometers (MSPs), which were distributed and situated beneath the auroral oval (Figure 1a, black dotted lines), Holmes et al. (2014) reexamined the nature of the shock aurora propagation at ionospheric heights. From MSP data distributed over different local time sectors, they confirmed that the occurrence of auroral emissions created by precipitating particles is observed to propagate tailward along the auroral oval with speeds of several kilometers per second, consistent with the shock propagation speed in the solar wind (Holmes et al., 2014).

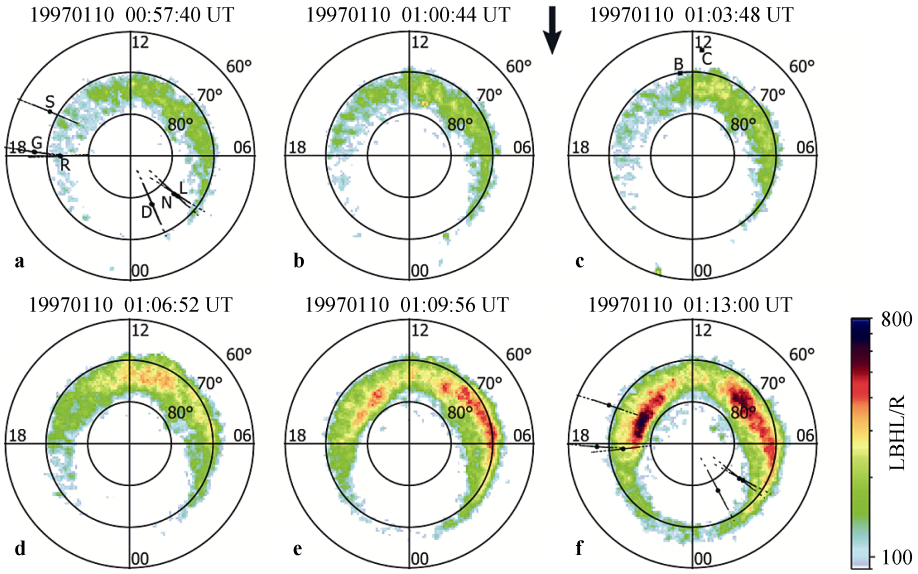

Figure 1 Shock aurora on 10 January 1997 as observed by Polar UVI LBHL images. A MLT/MLAT coordinate system is used with noon at the top and dusk on the left for each image. The black arrow marks the shock arrival; the onset of a shock aurora is first noted in the 01:06:52 UT image. Originally published by Zhou and Tsurutani (1999), and reproduced by Holmes et al. (2014).

A global intensification of the aurora was identified by the UVI on the Polar spacecraft (Brittnacher et al., 2000). After the arrival of the shock disturbance structure from a solar coronal mass ejection on 1 October 1997, the auroral luminosity was first observed to increase near local noon 2 min after the shock arrival, and a maximum intensity was achieved about 4 min later. Then intensification progressed rapidly along the dawn side within the first few minutes whereas a longer delay in the initial intensification was noted on the dusk side. Therefore, there is an asymmetry between the dawn side and dusk side in the arrival timing of the shock disturbance. Brittnacher et al. (2000) supposed that the effect of the pressure pulse associated with the shock structure at all local times is seen as an upward ramp in the energy flux that peaks earliest near the noon region. The ramp in precipitation energy has a steeper slope on the dusk side and peaks at a larger value than on the dawn side. They interpreted it as a broadening of the aurora to lower latitude of 71° MLAT and the subsequent peak intensity could be explained by the increase in the dayside region 1 FAC because the magnetopause was compressed.

Using global auroral images acquired by the UVI on board the Polar spacecraft, Liou et al. (2007) found that the luminosity of the aurora showed a general prompt and longer lasting increase in the dawn and dusk flanks of the oval in response to large solar wind dynamic pressure. This auroral activity is closely related with the compression state of the magnetosphere and is therefore termed a "compression aurora". The auroral oval is much wider during compression regardless of the sign of IMF B_z. The auroral luminosity increase may persist as long as the solar wind dynamic pressure stays high and may disappear ~10 min after the dynamic pressure drops. Meanwhile, global images of the proton aurora taken with the SI-12 camera onboard the IMAGE satellite (acronym for Imager for Magnetopause-to-Aurora Global Exploration) revealed a very direct relationship between increases in solar wind dynamic pressure and rises in intensity of the global proton aurora. A dawn–dusk asymmetry with the higher intensity at dusk was observed in the high dynamic pressure of solar winds, this intensity asymmetry being more dramatic under southward IMFs (Laundal and Østgaard, 2008).

There is another type of auroral response to IP shock compression, namely, the rapid response. This type of auroral emission appears almost simultaneously (within a few minutes) from dayside to nightside after the arrival of IP shock on the magnetopause (Chua et al., 2001; Hong et al., 2001; Su et al., 2011). Observations from satellite imagers show a comprehensive brightening over broad areas of the dayside and nightside aurora in response to an IP shock, indicating that more magnetospheric regions participate as sources for auroral particle precipitation than during isolated geomagnetic activities, such as auroral substorms. Calculations show that the rapid response may be linked with the propagation of the fast-mode wave at speeds of order 1000 km·s^{-1} in the magnetosphere launched by IP shocks (Moore et al., 1987). Using auroral data obtained by the IMAGE FUV-SI12 and FUV-SI13 imagers on 7 November 2004, Su et al. (2011) investigated one auroral intensification event induced by a strong IP shock. From this event, they found that protons (rather than electrons) were the dominant auroral precipitation component, and proton auroral intensification expanded longitudinally to the nightside sector within 2 min.

In addition to rapid and slower responses in the auroral oval, one particularly interesting new discovery is the

presence of lower latitude auroral arcs associated with IP shock or large solar wind pressure pulse. These auroral arcs have been described as midday sub-auroral patches (Liou et al., 2002), dayside subauroral proton flashes (Hubert et al., 2003), dayside detached aurora (Zhang et al., 2003; Zhou et al., 2018), and detached proton arcs (Immel et al., 2002). All of these descriptive terms identify common morphological features of the phenomenon. In particular, the arcs occur equatorward of and separate from the nominal auroral oval, and they are created entirely from precipitation of protons (Immel et al., 2002; Liou et al., 2002; Hubert et al., 2003; Zhang et al., 2003; Fuselier et al., 2004; Zhou et al., 2018). Midday sub-auroral patches are associated notably with both proton and electron precipitations of the diffuse-type (Liou et al., 2002). To date, Liou et al. (2002) is probably the first and only one to show an equatorward extension of the dayside aurora upon IP shock compression.

With observational data obtained from the coordinated DMSP and POES satellites, run by the US Department of Defense, Zhou et al. (2018) suggest that typical dayside detached aurora arcs are caused by solar wind pressure enhancement. As the IP shock compressed the magnetopause, the DMSP F18, F16, and F17 satellites flew over the Northern Hemisphere one after the other. Figure 2 gives the LBH short band (LBHS: 140.0–150.0 nm) and LBH long band (LBHL: 160.0–171.5 nm) images. Figure 2b exhibits a detached aurora that occurred at the dawn side and was separated by ~5° magnetic latitude (MLAT) from the equatorward edge of the northern auroral oval. This detached aurora was captured by the DMSP F16/SSUSI at 11:06 UT, just 2 min after the IP shock hit the magnetosphere (11:04). It expanded across a few degrees in MLAT within 60°–65° and extended from 0530 to 0830 magnetic local time (MLT). Figure 2c shows that, after a few minutes, at ~11:12 UT, the detached arc disappears signifying that the detached aurora emission might persist for less than 6 min. Furthermore, multiple-event studies demonstrated that detached aurora is usually very dynamic and short-lived with a lifetime of about 10 min (Zhang et al., 2003, 2004).

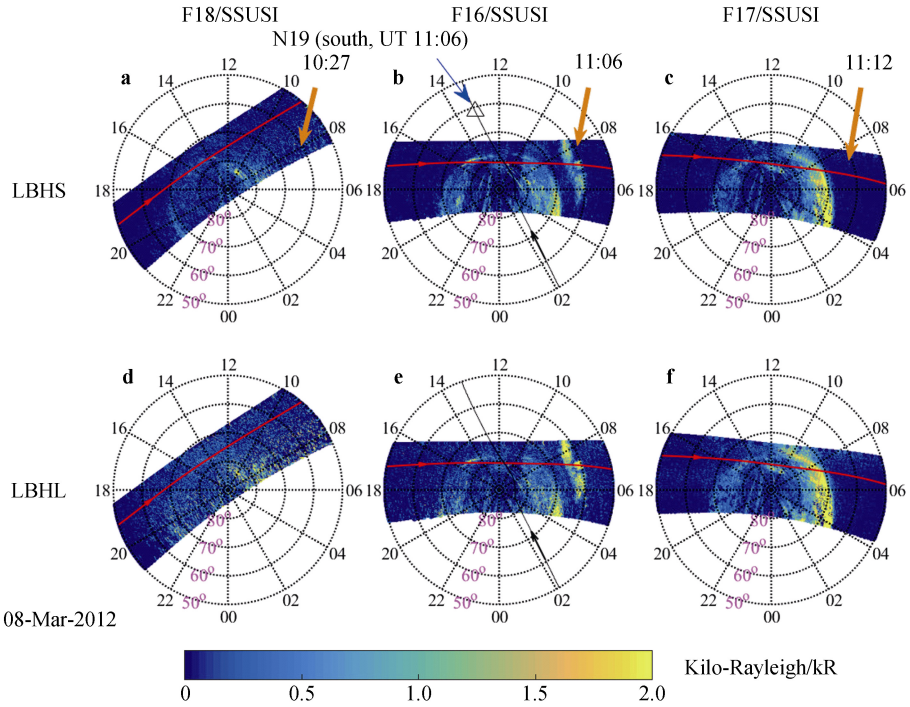

Figure 2 A series of Northern Hemisphere auroras observed by DMSP F18/SSUSI (**a** and **d**), F16/SSUSI (**b** and **e**) and F17/SSUSI (**e** and **f**) on 8 March 2012. These images are plotted in magnetic coordinates with magnetic latitude of 50°, 60°, 70° and 80°. The top (**a**–**c**) and bottom (**d**–**f**) three images show the LBHS (140–160 nm) and LBHL (160–180 nm), respectively. An auroral arc, separated from the auroral oval and indicated by a yellow arrow, can be seen from (**b**) and (**e**). The red and black lines show the footprints of the DMSP and POES satellites (Zhou et al. 2018).

3 Ground-based observations

Large-scale aurora imaging can reveal the overall solar wind-magnetosphere-ionosphere interaction process, but detailed ground-based measurements also play an essential role in understanding the fine interaction inside the magnetosphere–ionosphere coupled system. Egeland et al. (1994) obtained a pre-noon auroral intensity signature from ground MSP observations near the time of a SC triggered by an IP shock. The optical instrument monitored a series of auroral arcs spaced at ~1.1° intervals along magnetic latitude before the SC onset. During the SC, the entire sky was brightened with enhanced red 630.0-nm emissions extending from the northern horizon to south of the magnetic zenith,

whereas intense spatially separated green 557.7-nm emissions dominated the southern horizon. Dynamic Explorer 2 measured enhanced particle precipitation and sudden diminished convection in the morning sector. The auroral emissions became very weak ~20 min later. At almost the same time, Sandholt et al. (1994) noticed that a sharp enhancement in solar wind dynamic pressure ($\delta p/p \geqslant 0.5$) gave rise to equatorward shifts of the cusp aurora, and distinct ground magnetic signatures of enhanced ionospheric convection. They also found a sequence of auroral events of ~5–10-min recurrence times moving eastward along the poleward boundary of the persistent cusp aurora in the ~10–14 MLT sector during negative IMF B_z and B_y.

With coordinated observations from the ground-based TV all-sky camera (ASC), EISCAT, Super Dual Auroral Radar Network (SuperDARN) radars, and IMAGE FUV, Kozlovsky et al. (2005) investigated the dynamics of the dayside aurora oval associated with a SI triggered by the solar wind pressure pulse. Simultaneous ground-based and satellite observations allowed them to examine the response of high latitude auroral forms on a fine scale. After the SI, the center of the dayside auroral oval moved poleward from ~70° to 73° MLAT. This poleward motion was first seen in the 15-MLT sector. Later, it occurred in the MLT sectors located more westerly, ultimately reaching 6 MLT. The calculated velocity of the auroral disturbance propagating westward from 15 to 6 MLT was about 7 $km \cdot s^{-1}$. This motion of the middle of the auroral oval was suggested to be caused by the redistribution of the luminosity within the auroral oval and was not accompanied by a corresponding motion of the poleward boundary of the auroral oval. Detailed auroral observations near Svalbard (at ~11 MLT) showed evident brightening of the dayside auroral oval, and poleward moving auroral forms (rayed arcs) developed in the prenoon sector at 74°–76° MLAT. Radar observations showed that the SI was followed by an increase in the northward plasma drift velocity from ~50 $m \cdot s^{-1}$ to 550 $m \cdot s^{-1}$.

One detailed examination of the shock aurora occurred on 14 June 2005, see Figure 3 (Motoba et al., 2009). Ground-based optical observations at two wavelengths with

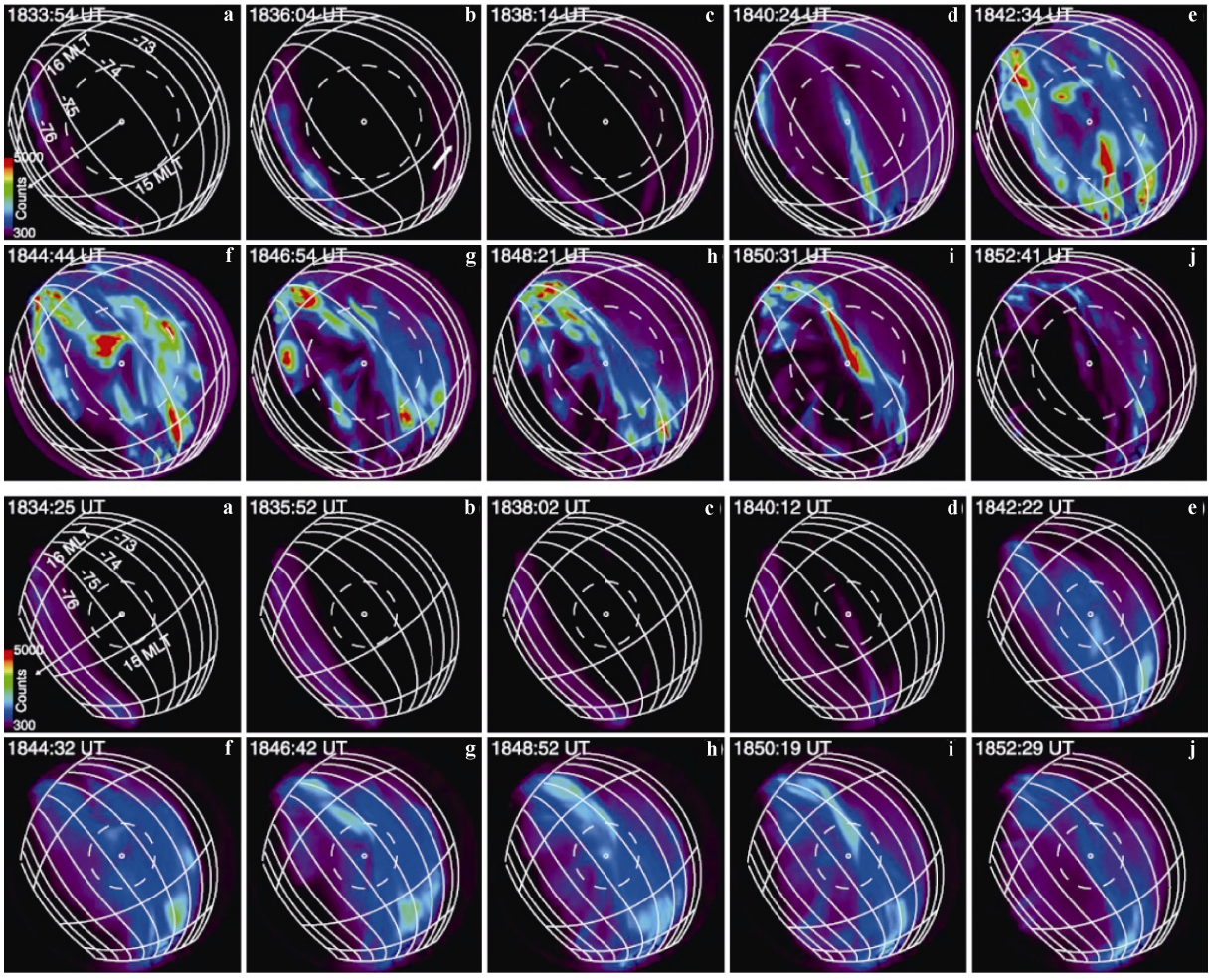

Figure 3 Top ten frames are sequence of all-sky images at 557.7 nm taken with the ASI at the South Pole Station. Selected geomagnetic latitude and MLT grid curves are overlaid. The direction to the magnetic pole is marked by thin arrow. Thick arrow in the second frame shows the initial brightening of diffuse emission. The bottom ten frames are sequences of all-sky images at 630.0 nm (Motoba et al., 2009).

high temporal and spatial resolution were taken with ASCs at the South Pole Station (SP, MLAT=−74.3°, MLT=UT−3.5 h), which were able to identify when and where diffuse and discrete-type aurora forms develop in the afternoon sector. From coordinated geomagnetic field observations, the major findings of the post-noon shock aurora for this case study included: (1) two-step development of the post-noon shock aurora—a diffuse-type shock aurora first appeared (marked by a white arrow in the first row of Figure 3) and expanded, and about 5 min later a discrete aurora began to develop; (2) this diffuse-type shock aurora was detectable only at 557.7 nm equatorward of the auroral oval (−70°–73° MLAT), while the discrete type at both 557.7 nm and 630.0 nm in the middle of the auroral oval (−73°–76° MLAT); and (3) the discrete arcs developed with relatively brighter emissions, and had a lifetime of about 10 min during the main phase of SC triggered by the IP shock.

Subsequently, Motoba et al. (2014) reported that the fine-scale transient aurora arcs were observed at SP, which emerged successively within the initial 1–2-min evolutionary interval of a post-noon shock aurora on 14 July 2012. Impressively, optical data were acquired from ~2 Hz temporal resolution imaging of the dayside aurora with a white-light ASC (Ebihara et al., 2007) and supplied fruitful optical data to reveal details of the evolution of the shock aurora. Just after SC onset, the ASC observed three successive transient arcs, the locations of which shifted equatorward with an abrupt jump by ~0.2° in latitude. Moreover, as inferred from the intensity ratio of $I_{630.0}/I_{557.7}$, all of the transient arcs occurred in the closed-field line region, ~1.0°–1.5° equatorward of the polar cap or the open/closed field line boundary but just poleward of the shock-induced proton and the diffuse-type electron aurorae. Each of the transient arcs had a latitudinal width of ~0.1° and a short lifetime of ~20–30 s. In other words, the new arc appeared equatorward of the preceding arc with a latitudinal separation of ~0.2°, with the preceding arc decaying just after the appearance of the new arc.

Ground-based imager observations of a shock aurora event were also reported by Zhou et al. (2009). This event was well observed by optical instruments with green (557.7 nm) and red (630.0 nm) line emissions when the observatory located in Svalbard was at ~1120 MLT close to magnetic local noon. The ground-based imager supplied 30-s resolution data and gave an excellent opportunity to investigate the direct response of the optical aurora to an external shock impact. The imager detected an auroral intensification by a factor of two or more in both green and red line emissions within 5 min after the shock arrival at the magnetopause. The intensified green emissions were mainly from a diffuse-type aurora on closed field lines. They were latitudinally below and adjacent to the red aurora in higher latitude region, and were mainly in the form of arcs and beams along the magnetic east-west direction. The diffuse aurorae were noted to expand equatorward and eastward, and its intensity exceeded the red arcs. In addition, the eastward propagation of the aurora along the auroral oval suggests that the anti-sunward-propagating shock aurora seen in space from satellite observations is mainly diffuse aurora. Moreover, the azimuthal motion of the diffuse aurora presented by Zhou et al. (2009) is opposite to western expanding aurora reported by Kozlovsky et al. (2005). Both IMAGE global auroral images and ground-based ASI observed that western expanding aurora in the dayside oval is actually a discrete aurora, but the eastward-propagating aurora measured by ASI is a uniform diffuse aurora.

Most of the studies on satellite-observed and ground-based optical aurora noted the general increase in the auroral intensity in response to IP shocks, which at first instinct is expected because of the sudden external squeezing-induced intense energetic particle precipitation. However, using ASC data taken at 4-s intervals at the Chinese Zhongshan Station (ZHS, −74.5 MLAT, MLT=UT+1.5 h) in Antarctica (He et al., 2016), Liu et al. (2011) first reported an initial diminishing of the auroral luminosity because of the IP shock. Figure 4 present a sequence of auroral snapshots taken post-noon at one-minute intervals from ZHS and simultaneous optical data (right panel) in the pre-noon sector at SP. The SC onset identified by the geomagnetic field observation and marked in the third frame of each panel was at ~1458 UT. Figure 4a shows an aurora in the arc and ray structures with moderate luminosity before the IP shock arrival seen in the poleward direction of the field of view (FOV) at 1457 UT and 1458 UT, and may reflect the localized background particle precipitation at that time. After the SC onset from 1459 to 1502 UT, the auroral intensity over ZHS had decreased significantly with the images showing just dim visible remnants in the FOV of the ASC frame. Figure 4a shows that at 1503 UT (4 min after SC onset), an auroral arc with intense brightness appears visible noticeably near the zenith of ASC at ZHS. With the associated auroral arc gradually moving equatorward, the entire sky brightened accordingly.

Figure 4b presents the optical white-light auroral observation over SP, the time sequence being completely identical with that of Figure 4a. Note that SP has nearly the same magnetic latitude as ZHS and was located in the pre-noon (~1100 MLT) sector at the SC time. The impressive feature present in Figure 4b is the prompt auroral brightening at 1459 UT, which is just after the SC onset. The auroral luminosity over SP increased considerably from 1459 to 1502 UT, indicating a significant enhancement of the energetic particle precipitation in the pre-noon sector. Thus, the optical aurora features observed at SP in the pre-noon sector were just opposite to those captured at ZHS in the post-noon sector.

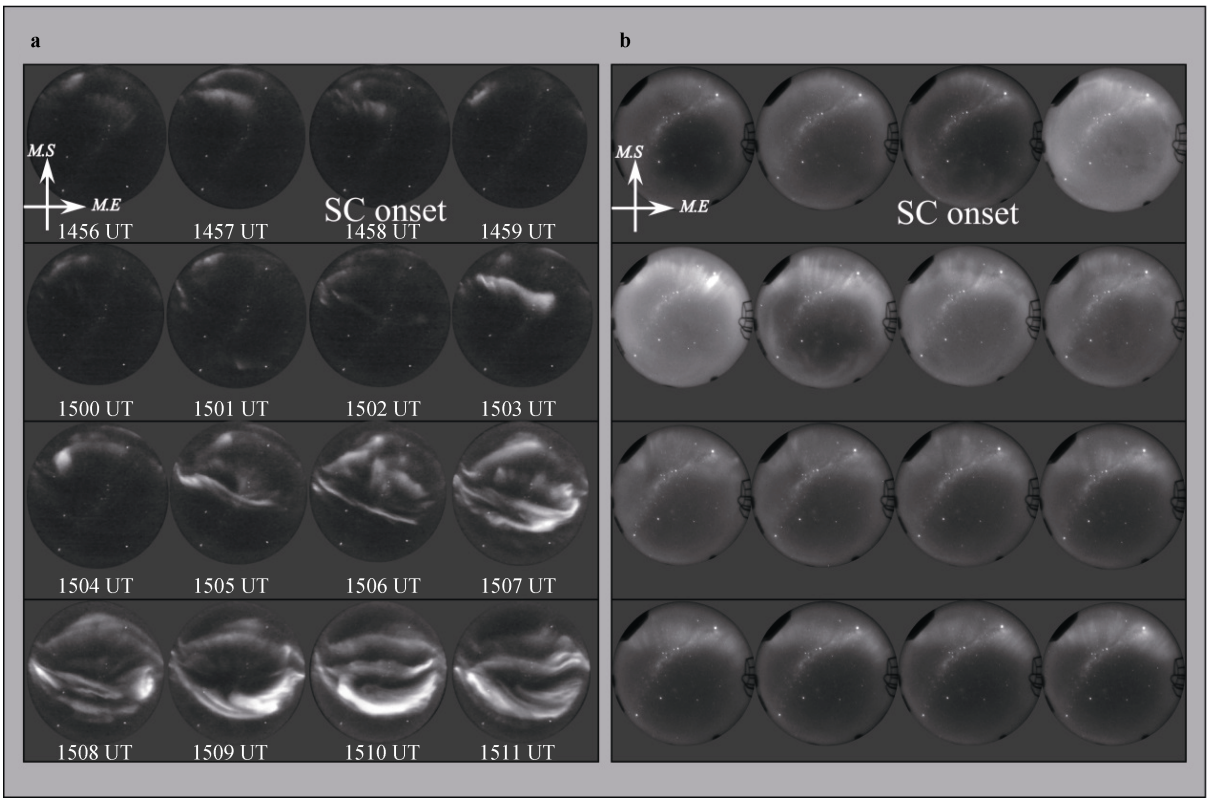

Figure 4 Auroral all-sky images taken with Zhongshan Station (**a**) and South Pole Station (**b**) during 1456–1511 UT. The geomagnetic directions are marked in the first frame. *M.S* and *M.E* indicate the magnetic south and magnetic east directions, respectively (Liu et al., 2011).

Comparison results from the SuperDARN radar of high temporal aurora and the global geomagnetic observations showed that auroral diminishing in the post-noon sector corresponds to a flow reversal of ionospheric plasma from sunward to anti-sunward within nearly the same time period. Geomagnetic field variations point to a plasma flow reversal, an auroral diminishing post-noon, and an auroral increase pre-noon occurring in the preliminary phase of the SC (Figure 5). As the main factor generating auroral arcs, precipitating particles are well-known as having a close relationship with the FACs. The up-moving electrons have been identified as the main carriers of downward FACs (Klumpar and Heikkila, 1982; Burch et al., 1983). In addition, Marklund et al. (1994) found up-moving electrons were associated with black aurora in the downward FAC region and indicated that a total absence of auroral emission was caused by up-moving electron beams carried by a downward FAC. Therefore, the auroral decrease observed over ZHS at the initial stage of SC is mostly caused by a downward FAC that was produced by the interaction of the IP shock with the magnetosphere. However, the SuperDARN radar, a successful tool in geospace for determining FACs through its convection observations, provided convincing evidence for the formation of a downward FAC over ZHS during the auroral diminishing interval (Bristow and Lummerzheim, 2001; Chisham et al., 2007; Lester, 2008). Rapidly reversed ionospheric plasma flow measured by SuperDARN gave strong evidence of the formation of a downward FAC just after the SC onset.

Afterwards, a dusk shock aurora event was reported based on simultaneous optical and SuperDARN radar observations over ZHS (Liu et al., 2013). A new thin aurora arc with brighter emissions and subsequent auroral vortices was formed during the main phase of the SI triggered by an IP shock. Auroral vortices are typically measured by ground-based ASI (Connors and Rostoker, 1993), and such structures were associated with plasma waves in the magnetospheric dusk or dawn boundary layer (Wei and Lee, 1993).

Using optical aurora observations with high temporal and spatial resolution, Liu et al. (2015) investigated one fortuitous event that illustrated the direct responses of the fine structure auroral emissions to IP shocks. During the shock impact on the magnetosphere, the Chinese Arctic Yellow River Station (YRS) equipped with ASIs was situated at the magnetic local noon region (~1210 MLT) in the Northern Hemisphere (Han et al., 2018). An intensified red aurora manifesting as a discrete emission band at higher latitude was observed to respond to the shock impact gradually. Equatorward shifting of the red aurora resulted in a distinct broadening of the dayside auroral oval after the IP

shock arrival. In contrast, the green diffuse aurora, manifesting as a relatively uniform luminosity structure, reacted immediately to the shock compression, displaying a prompt appearance in the southern edge of the FOV and subsequent poleward propagation of its higher latitude boundary.

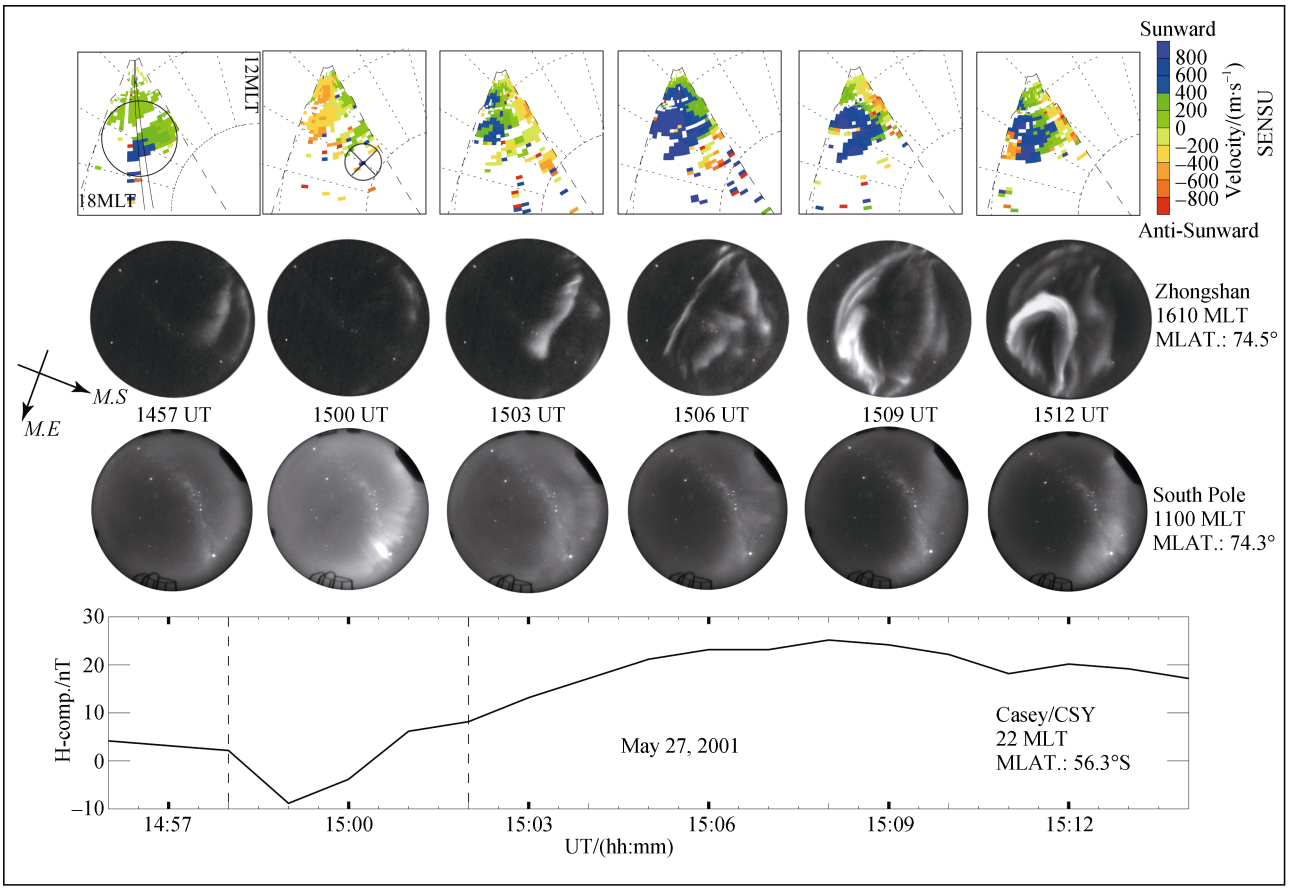

Figure 5 Line of sight (LOS) velocities between 1457 and 1512 UT with 3 min intervals observed by SuperDARN Syowa East radar, simultaneous auroral images over Zhongshan and South Pole stations, and the geomagnetic horizontal H component at Mawson (Liu et al., 2011).

4 Main production mechanisms

Next, we attempt to outline the major known mechanisms that may be responsible for the generation or intensification of the shock aurora in the solar wind–magnetosphere coupled system. Several different mechanisms are possible that may be taking place simultaneously in a certain MLT sector. In theory, different physical mechanisms contribute to different auroral forms, and therefore we try to give some related auroral forms.

4.1 Adiabatic compression

It is known that the increased auroral intensity and energetic electron precipitation coincide with changes in magnetic field line geometry caused by the IP shock sudden compression. The effect was first identified when accounting for electron energization and their mirroring deeper in the atmosphere than that before IP shock compression (Spann et al., 1998); the second was in observing a more uniform magnetic fields near the equator, which allowed the electrons and whistler wave to remain in gyro-resonance for longer intervals, thereby reducing the mirror ratio (Liou et al., 2007).

A physical model for the auroral brightening and rapid propagation in polar ionosphere was proposed by Zhou and Tsurutani (1999). For an IP shock incident normal to the magnetopause, the compressional wave initially occurs at the magnetopause nose (~12 MLT) and then expands towards the dawn and dusk flanks as the shock wave moves to the magnetotail region. Assuming a conserved first adiabatic invariant of the trapped plasma, Zhou et al. (2003) developed their model by examining coordinated large-scale aurora and *in-situ* wave-particle observations carried by the wave analyzer onboard the FAST satellite. A schematic of the adiabatic compression model (Figure 6) shows that the increase in ram pressure across the shock compresses the frontside magnetosphere. Compression of the outer magnetospheric field lines leads to an increase in perpendicular kinetic energy ($E_{\perp}$) of the electrons (and protons) on those field lines, resulting in a

temperature anisotropy ($T_{\perp} / T_{\parallel} > 1$). A loss cone instability occurs that then leads to the growth of a plasma wave such as the electromagnetic whistler-mode wave (Tsurutani et al., 1998). The growth of the electromagnetic whistler mode wave scatters particles into the loss cone (Tsurutani et al., 2001).

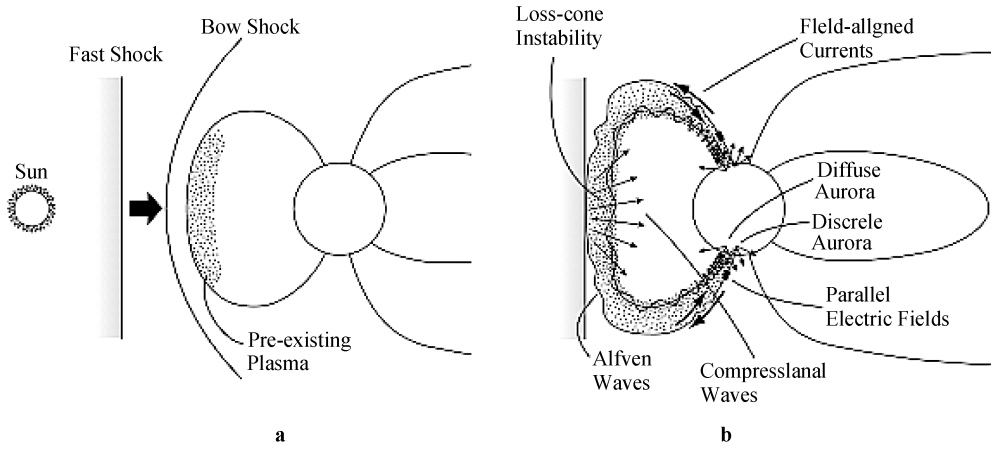

Figure 6 Schematic of possible phenomena in the dayside magnetosphere and ionosphere that are generated by IP shock or solar wind pressure pulses compression (Zhou et al., 2003).

During magnetospheric compression events, Anderson and Hamilton (1993) noticed enhanced electromagnetic ion cyclotron waves and Lauben et al. (1998) also noted increased electromagnetic whistler-mode chorus emissions. These results support the above scenario for the onset of dayside cone instabilities of proton and electron loss during shock compression events. Moreover, satellite and ground-based observational measurements of aurora have provided direct evidence for these intensified electromagnetic waves (Zhang et al., 2008; Shi et al., 2012, 2014).

Regarding the detached dayside aurora (DDA), both the IMAGE and DMSP data confirmed that DDA are separated from the dayside auroral oval, and hence Zhang et al. (2003) advised that the particle source of DDA is very likely to be in the dayside ring current, located in the region L=2–9. Using rare in-situ Polar proton EMIC wave and simultaneous satellite auroral observations, Zhang et al. (2008) investigated an IP shock-induced DDA. Observational results and ring current simulations show that sudden bursts of proton EMIC waves are closely related to the DDA, and ~10-keV protons with a sausage-shaped spatial distribution of high anisotropy in flux and temperature were the particle source for the dusk side and nightside detached aurora (Zhou et al., 2018).

Electrons lost into the loss cone through adiabatic compression as described above precipitate into the polar atmosphere along magnetic field lines the foot-prints of which are uniform in the atmosphere. When the precipitating energy flux is high enough, aurorae are generated and have been seen as a structureless bright background, i.e., diffuse aurora (Zhou et al., 2003, 2009; Motoba et al., 2009; Han et al., 2015; Liu et al., 2015).

Magneto-spherical plasma and the magnetic field associated with an IP shock or the solar wind dynamic pressure enhancement were investigated extensively by satellite measurements (Baumjohann et al., 1983; Samsonov et al., 2007). After the SI, the magnetic field changes were mainly compressional in the preliminary phase of the geomagnetic disturbance (Araki, 1994). Multiple-event studies demonstrated that significant changes take place in the auroral oval location, side, and intensity in response to the IP shock compression (Boudouridis et al., 2003). Prominent features are an increase in the auroral oval width, a decrease in the polar cap size, and an enhanced total precipitating particle energy flux.

4.2 FAC intensifications

The shock compression of the magnetosphere leads to a profound and complicated disturbance of the FACs (Araki, 1994; Nishimura et al., 2016). Typically, the compression effect appears in the dayside centered on the shock impact location where the low-latitude magnetopause is displaced the most by the prompt compression. The compressional waves propagate earthward, and the coupling of the compressional waves with the kinetic Alfvén waves suggests the formation of a pair of FACs and corresponding ionospheric vortices around local noon. The ground signature of the FACs arising from the IP shock or solar wind pressure pulses are described as geomagnetic disturbance at low and high latitudes (DL and DP). The DP disturbance is composed of a sharp preliminary impulse (PI) of short duration and a subsequent main impulse (MI). Generally, the polarity of the FACs is opposite for PI and MI, but the strength is more intense for MI. From ground magnetometers, the pair of FACs is directed into and out of the polar ionosphere. DP_{pi} field-associated FACs flow into (out of) the afternoon (morning) polar ionosphere, whereas the DP_{mi} field-associated FACs flow in the opposite direction to that of the DP_{pi}.

When the IP shock interacts with the magnetosphere, a compressional wave front has been suggested to propagate within the inhomogeneous magnetosphere and can convert to an Alfvén wave carrying FACs for PI (Araki, 1994). A numerical simulation showed that the PI-related FAC is converted from the cross-field current in regions with steep Alfvén velocity gradient, whereas the main impulse-associated FAC (flowing into the dawn and out of the dusk polar ionosphere) is generated from an enhanced dawn–dusk-directed magnetospheric convection electric field (Fujita et al., 2003a, 2003b). Samsonov et al. (2010) found that following a strong IP shock the enhanced FACs are related strongly to the dynamo region near the equatorial plane on the magnetospheric dawn and dusk flanks. The existence of the dynamo near the flanks that power the MI-related FACs was confirmed by MHD simulation (Sun et al., 2015). The generation of the unstable FACs is a process that converts energy stored in the magnetic shear stresses initiated from the shock compression into kinetic energy (Zhou et al., 2003).

Satellite *in-situ* observations show that the downward electron flux is significantly high along the upward FACs but is low between the upward FACs layers, where the currents are going downward (Zhou et al., 2003). Therefore, the aurora generated beneath the upward FAC layers is much brighter than that beneath the downward currents. Because the upward FAC layers are very thin in the magnetic latitudinal directions, the aurora beneath them looks like discrete brightenings or arcs in the polar ionosphere that outline the footprint of the upward FACs. Although the electrons precipitated along the upward FACs are at low energies (< ~1 keV), this does not necessarily imply a low auroral intensity because the aurora luminosity is determined by the strength of the energy flux instead of the energy level of the individual electrons. In this way, the auroral arcs can be very distinguishable by their noticeable forms. These observed optical signatures from a ground-based ASC contain discrete shock aurora in higher latitude region manifesting as multiple arcs (Motoba et al., 2009; Liu et al., 2011, 2013; Zhou et al., 2017). A schematic representation of the enhanced FACs associated with an IP shock compression is illustrated in Figure 6b, which is believed to be a discrete type of auroral beam, arc or ray in the higher latitude of the dayside auroral oval.

4.3 Flow shearing

On the magnetopause, the sudden compression caused by the enhanced solar wind dynamic pressure produces magnetic perturbations and waves (Ogilvie and Fitzenreiter, 1989; Rae et al., 2012). Geomagnetic field disturbances indicate that the ionospheric plasma flow shear can launch Kelvin–Helmholtz (KH) instabilities (Kozlovsky et al., 2005). The growth rates for the KH instability maximize flow shears perpendicular to the magnetic field. Such shears occasionally occur at the magnetopause and frequently occur at the inner edge of the low-latitude boundary layer. Perturbations on the magnetopause during IP shock propagation develop naturally into kinetic waves. Corresponding rolled-up vortices mapped along the geomagnetic field lines have also been detected in satellite large-scale and ground-based auroral arcs (Connors and Rostoker, 1993; Hu et al., 2013; Liu et al., 2013). Vorticity associated with waves in the dusk (dawn) boundary layer generates localized upward (downward) FACs into both the northern and southern polar ionospheres. Discrete aurora in beads or spirals and the SC-associated geomagnetic pulsations in both the dawn side and dusk side high-latitude ionosphere have been attributed to the KH instability driven by a fast shocked solar wind (Connors and Rostoker, 1993; Hu et al., 2013).

Because of ionospheric Joule dissipation, these aurora vortices should survive less than ~10 min. The vortices travel tailward with the phase velocity of an unstable KH wave triggered by an IP shock compression, which is nearly equal to half the magnetosheath flow speed (Connors and Rostoker, 1993). Structured auroral forms are closely correlated with velocity shearing between the magnetosheath and the lower latitude boundary layer. Therefore, the growth rates for the KH instability are maximized for flow shears during IP shock passage by the magnetospheric cavity. During magnetospheric compressing, the plasma flow in the magnetosheath has a larger velocity with anti-sunward flow along the flanks at dawn and dusk, whereas the convective return flow dominates in the inner lower latitude magnetosphere. Consequently, a viscous interaction was invoked and then involved in the transfer of momentum from the solar wind to a closed field line region just inside the boundary. Therefore, a distinguished pearl or spiral aurora in the morning and afternoon polar ionosphere was caused by the KH instability (Hu et al., 2013; Johnson et al., 2014).

5 Summary and outlook

Ground-based shock aurora in the dawn side and dusk side generally present some similar feature in form such as sequential transient arcs separated at ~1.0º intervals in MLAT embedded within a FAC system. In regard to the different types of shock-aurora forms, discrete aurora manifesting as a sharp structure with roughly east–west aligned arcs, beams or corona usually occur in the higher latitude region, whereas diffuse aurora as a uniform luminous structure conventionally dominate the southern region relative to the normal auroral oval and occasionally overlap with the discrete aurora.

We have argued that there is significant energetic particle precipitation that occurs within the dayside auroral zone during shock compression. Preliminary mechanisms for particle energization and precipitation were introduced. High temporal and spatial resolution ground-based imaging data will be extremely useful in resolving issues regarding the mechanisms that operate in reality and which are the

most effective. Nonetheless, energetic particle and wave measurements at higher altitude are needed to identify the in-situ primary physical process. Moreover, capturing the fine shock auroral structure and forms for identifying discrete and diffuse-type aurora is necessary because different auroral forms correspond to different energetic precipitation source regions and certain plasma waves. In such cases, we suggest several issues should be investigated in the near future:

(1) Using optical measurements performed by China's Auroral Fine-structure Imaging System at Zhongshan Station (Liu et al., 2008), detailed evolution of the shock aurora in different forms and multiple scales could be investigated to reveal the associated FACs.

(2) Given the superior geomagnetic location of the Chinese Yellow River Station, and because it is situated just under the auroral oval when the station rotates around the magnetic local noon region, more attention should be focused on the precise response sequence of different wavelengths to check the dominance of the FACs and wave–particle interaction from both discrete and diffuse aurorae.

(3) Coordinated with measurements by the SuperDARN, shock-aurora associated ionospheric localized convection near the magnetic noon should be examined in detail because shock-triggered FACs could generate ionospheric traveling convection vortices, which could be monitored by a combination of optical auroral and SuperDARN observations.

Acknowledgments This work was supported by the NSFC (Grant nos. 41431072, 41674169, 41474146, and 41831072), the International Collaboration Supporting Project by the Chinese Arctic and Antarctic Administration (Grant no. IC201608), the National Key R&D Program of China (Grant no. 2018YFC1407304), and the Chinese Meridian Project. The authors acknowledge the use of SuperDARN data. SuperDARN is a collection of radars funded by national scientific agencies of Australia, Canada, China, France, Italy, Japan, Norway, South Africa, UK, and the United States of America.

References

Anderson B J, Hamilton D C. 1993. Electromagnetic ion cyclotron waves stimulated by modest magnetospheric compressions. J Geophys Res-Space, 98: 11369-11382, doi: 10.1029/93JA00605.

Araki T. 1994. A physical model of the geomagnetic sudden commencement. Geophys Monogr Ser, 81: 183-200.

Axford W I, Hines C O. 1961. A unifying theory of high-latitude geophysical phenomena and geomagnetic storms. Can J Phys, 39: 1433-1464.

Baumjohann W, Bauer O H, Haerendel G, et al. 1983. Magnetospheric plasma drifts during a sudden impulse. J Geophys Res-Space, 88: 9287-9289, doi: 10.1029/JA088iA11p09287.

Boudouridis A, Lyons L R, Zesta E, et al. 2007. Dayside reconnection enhancement resulting from a solar wind dynamic pressure increase. J Geophys Res-Space, 112: A06201, doi: 10.1029/2006JA012141.

Boudouridis A, Lyons L R, Zesta E, et al. 2008. Nightside flow enhancement associated with solar wind dynamic pressure driven reconnection. J Geophys Res-Space, 113: A12211, doi: 10.1029/2008JA013489.

Boudouridis A, Zesta E, Lyons R, et al. 2003. Effect of solar wind pressure pulses on the size and strength of the auroral oval. J Geophys Res-Space, 108(A4): 8012, doi:10.1029/2002JA009373.

Bristow W A, Lummerzheim D. 2001. Determination of field-aligned currents using the Super Dual Auroral Radar Network and the UVI ultraviolet imager. J Geophys Res-Space, 106(A9): 18577-18587.

Brittnacher M, Wilber M, Fillingim M, et al. 2000. Global auroral response to a solar wind pressure pulse. Adv Space Res, 25: 1377-1385.

Burch J L, Reiff P H, Sugiura M. 1983. Upward electron beams measured by DE-1: A primary source of dayside region-1 birkeland currents. Geophys Res Lett, 10: 753-756.

Chisham G, Lester M, Milan S E, et al. 2007. A decade of the Super Dual Auroral Radar Network (SuperDARN): scientific achievements, new techniques and future directions. Surv Geophys, 28: 33-109.

Chua D, Parks G, Brittnacher M, et al. 2001. Energy characteristics of auroral electron precipitation: A comparison of substorms and pressure pulse related auroral activity. J Geophys Res-Space, 106: 5945-5956.

Connors M, Rostoker G. 1993. Source mechanisms for morning auroral features. Geophys Res Lett, 20: 1535-1538.

Dungey J W. 1961. Interplanetary magnetic field and the auroral zones. Phys Rev Lett, 6: 47-48.

Ebihara Y, Tanaka Y-M, Takasaki S, et al. 2007. Quasi-stationary auroral patches observed at the South Pole Station. J Geophys Res-Space, 112: A01201, doi: 10.1029/2006JA012087.

Egeland A, Burke W J, Maynard N C, et al. 1994. Ground and satellite observations of postdawn aurorae near the time of a sudden storm commencement. J Geophys Res-Space, 99: 2095-2108.

Fujita S, Tanaka T, Kikuchi T, et al. 2003a. A numerical simulation of the geomagnetic sudden commencement: 1. Generation of the field-aligned current associated with the preliminary impulse. J Geophys Res-Space, 108(A12): 1416, doi:10.1029/2002JA009407.

Fujita S, Tanaka T, Kikuchi T, et al. 2003b. A numerical simulation of the geomagnetic sudden commencement: 2. Plasma processes in the main impulse. J Geophys Res-Space, 108(A12): 1417, doi:10.1029/2002JA009763.

Fuselier S A, Gary S P, Thomsen M F, et al. 2004. Generation of transient dayside subauroral proton precipitation. J Geophys Res-Space,109(A12): 227, doi: 10.1029/2004JA010393.

Gao Y. 2012. Comparing the cross polar cap potentials measured by SuperDARN and AMIE during saturation intervals. J Geophys Res-Space, 117: A08325, doi: 10.1029/2012JA017690.

Guo X C, Hu Y Q, Wang C. 2005. Earth's magnetosphere impinged by interplanetary shocks of different orientations. Chinese Phys Lett, 22: 3221.

Han D, Hu Z, Chen X, et al. 2018. Recents results obtained from dayside optical auroral observations at Yellow River Station. Chin J Polar Res, 30(3): 235-250.

Han D S, Araki T, Yang H G, et al. 2007. Comparative study of Geomagnetic Sudden Commencement (SC) between Oersted and ground observations at different local times. J Geophys Res-Space, 112: A05226, doi: 10.1029/2006JA011953.

Han D S, Chen X C, Liu J J, et al. 2015. An extensive survey of dayside diffuse aurora based on optical observations at Yellow River Station. J Geophys Res-Space, 120: 7447-7465, doi: 10.1002/2015JA021699.

He F, Hu H Q, Yang H G, et al. 2016. Recent progress in Chinese polar upper-atmospheric physics research: review of research advances supported by the Chinese Arctic and Antarctic expeditions. Adv Polar Sci, 27(4): 219-232, doi: 10.13679/j.advps.2016.4.00219.

Holmes J M, Johnsen M G, Deehr C S, et al. 2014. Circumpolar ground-based optical measurements of proton and electron shock aurora. J Geophys Res-Space, 119: 3895-3914, doi: 10.1002/2013JA019574.

Hong M, Wang X, Chua D, et al. 2001. Auroral substorm response to solar wind pressure shock. Chinese Sci Bull, 46: 1547-51.

Hu Z J, Yang H G, Hu H Q, et al. 2013. The hemispheric conjugate observation of postnoon "bright spots"/auroral spirals. J Geophys Res-Space, 118: 1428-1434, doi: 10.1002/jgra.50243.

Hubert B, Gérard J C, Fuselier S A, et al. 2003. Observation of dayside subauroral proton flashes with the IMAGE-FUV. Geophys Res Lett,30(3): 1145, doi: 10.1029/2002GL016464.

Immel T J, Mende S B, Frey H U, et al. 2002. Precipitation of auroral protons in detached arcs. Geophys Res Lett, 29(11): 141-144, doi: 10.1029/2001GL01384.

Johnson J R, Wing S, Delamere P A. 2014. Kelvin Helmholtz instability in planetary magnetospheres. Space Sci Rev, 184: 1-31.

Klumpar D M, Heikkila W J. 1982. Electrons in the ionospheric source cone: Evidence for runaway electrons as carriers of downward Birkeland currents. Geophys Res Lett, 9: 873-876.

Kozlovsky A, Safargaleev V, Østgaard N, et al. 2005. On the motion of dayside auroras caused by a solar wind pressure pulse. Ann Geophys, 23: 509-521.

Lauben D S, Inan U S, Bell T F, et al. 1998. VLF chorus emissions observed by POLAR during the January 10, 1997, magnetic cloud. Geophys Res Lett, 25: 2995-2998.

Laundal K M, Østgaard N. 2008. Persistent global proton aurora caused by high solar wind dynamic pressure. J Geophys Res-Space, 113: A08231, doi: 10.1029/2008JA013147.

Lester M. 2008. SuperDARN: An example of a network approach to geospace science in the twenty-first century. J Atmos Sol-Terr Phy, 70: 2309-2323.

Liou K, Newell P T, Shue J H, et al. 2007. "Compression aurora": Particle precipitation driven by long-duration high solar wind ram pressure. J Geophys Res-Space, 112: A11216, doi: 10.1029/2007JA012443.

Liou K, Wu C C, Lepping R P, et al. 2002. Midday sub-auroral patches (MSPs) associated with interplanetary shocks. Geophys Res Lett, 29: 181-184.

Liu J, Hu H, Han D, et al. 2013. Optical and SuperDARN radar observations of duskside shock aurora over Zhongshan Station. Adv Polar Sci, 24(1): 60-68, doi: 10.3724/SP.J.1085.2013.00060.

Liu J, Hu H, Han D, et al. 2015. Simultaneous ground-based optical and SuperDARN observations of the shock aurora at MLT noon. Earth, Planets and Space, 67: 120.

Liu J J, Hu H Q, Han D S, et al. 2011. Decrease of auroral intensity associated with reversal of plasma convection in response to an interplanetary shock as observed over Zhongshan Station in Antarctica. J Geophys Res-Space, 116: A03210.

Liu S, Han D, Hu H, et al. 2008. Prospect of China's Auroral Fine-structure Imaging System (CAFIS) at Zhongshan Station in Antarctica. Chin J Polar Sci, 19(2): 261-266.

Marklund G, Blomberg L, Fälthammar C-G, et al. 1994. On intense diverging electric fields associated with black aurora. Geophys Res Lett, 21: 1859-1862.

Meurant M, Gérard J C, Hubert B, et al. 2003. Dynamics of global scale electron and proton precipitation induced by a solar wind pressure pulse. Geophys Res Lett, 30(20): 2032, doi:10.1029/2003GL018017.

Moore T E, Gallagher D L, Horwitz J L, et al. 1987. MHD wave breaking in the outer plasmasphere. Geophys Res Lett, 14: 1007-1010.

Motoba T, Ebihara Y, Kadokura A, et al. 2014. Fine-scale transient arcs seen in a shock aurora. J Geophys Res-Space, 119: 6249-6255.

Motoba T, Kadokura A, Ebihara Y, et al. 2009. Simultaneous ground-satellite optical observations of postnoon shock aurora in the Southern Hemisphere. J Geophys Res-Space, 114: A07209, doi:10.1029/2008JA014007.

Nishimura Y, Kikuchi T, Ebihara Y, et al. 2016. Evolution of the current system during solar wind pressure pulses based on aurora and magnetometer observations. Earth, Planets and Space, 68: 1-16.

Ogilvie K W, Fitzenreiter R J. 1989. The Kelvin-Helmholtz instability at the magnetopause and inner boundary layer surface. J Geophys Res-Space, 94: 15113-15123.

Rae I J, Mann I R, Murphy K R, et al. 2012. Ground-based magnetometer determination of in situ Pc4–5 ULF electric field wave spectra as a function of solar wind speed. J Geophys Res-Space, 117: A04221, doi:10.1029/2011JA017335.

Samsonov A A, Sibeck D G, Imber J. 2007. MHD simulation for the interaction of an interplanetary shock with the Earth's magnetosphere. J Geophys Res-Space, 112: A12220, doi:10.1029/2007JA012627.

Samsonov A A, Sibeck D G, Yu Y. 2010. Transient changes in magnetospheric-ionospheric currents caused by the passage of an interplanetary shock: Northward interplanetary magnetic field case. J Geophys Res-Space, 115: A05207, doi: 10.1029/2009JA014751.

Sandholt P E, Farrugia C J, Burlaga L F, et al. 1994. Cusp/cleft auroral activity in relation to solar wind dynamic pressure, interplanetary magnetic field B_z and B_y. J Geophys Res-Space, 99: 17323-17342.

Shi R, Han D, Ni B, et al. 2012. Intensification of dayside diffuse auroral precipitation: contribution of dayside Whistler-mode chorus waves in realistic magnetic fields. Ann Geophys, 30: 1297-1307.

Shi R, Hu Z J, Ni B, et al. 2014. Modulation of the dayside diffuse auroral intensity by the solar wind dynamic pressure. J Geophys Res-Space, 119: 10092–10099, doi: 10.1002/2014JA020180.

Spann J F, Brittnacher M, Elsen R, et al. 1998. Initial response and complex polar cap structures of the aurora in response to the January 10, 1997 magnetic cloud. Geophys Res Lett, 25: 2577-2580.

Su Z, Zong Q G, Yue C, et al. 2011. Proton auroral intensification induced by interplanetary shock on 7 November 2004. J Geophys Res-Space, 116: A08223, doi: 10.1029/2010JA016239.

Sun T R, Wang C, Zhang J J, et al. 2015. The chain response of the magnetospheric and ground magnetic field to interplanetary shocks. J Geophys Res-Space, 120: 157-165, doi:10.1002/2014JA020754.

Tsurutani B T. 1998. The January 10, 1997 auroral hot spot, horseshoe aurora and first substorm: A CME loop? Geophys Res Lett, 25: 3047-3050.

Tsurutani B T. 2001. Interplanetary shocks,magnetopause boundary layers and dayside auroras: the importance of a very small magnetospheric

region. Surv Geophys, 22: 101-130.

Tsurutani B T, Arballo J K, Lakhina G S, et al. 1998. Plasma waves in the dayside polar cap boundary layer: Bipolar and monopolar electric pulses and whistler mode waves. Geophys Res Lett, 25: 4117-4120.

Tsurutani B T, Lakhina G S, Verkhoglyadova O P, et al. 2011. A review of interplanetary discontinuities and their geomagnetic effects. J Atmos Sol-Terr Phy, 73: 5-19.

Tsurutani B T, Zhou X Y, Arballo J K, et al. 2001. Auroral zone dayside precipitation during magnetic storm initial phases. J Atmos Sol-Terr Phy, 63: 513-522.

Wei C Q, Lee L C. 1993. Coupling of magnetopause-boundary layer to the polar ionosphere. J Geophys Res-Space, 98: 5707-5725

Zesta E, Lyons L R, Donovan E. 2000. The auroral signature of Earthward flow bursts observed in the Magnetotail. Geophys Res Lett, 27(20): 3241-3244.

Zhang Y, Paxton L J, Immel T J, et al. 2003. Sudden solar wind dynamic pressure enhancements and dayside detached auroras: IMAGE and DMSP observations. J Geophys Res-Atmospheres, 108(A4): 8001, doi: 10.1029/2002JA009355.

Zhang Y, Paxton L J, Meng C I, et al. 2004. Double dayside detached auroras: TIMED/GUVI observations. Geophys Res Lett, 31: L10801.

Zhang Y, Paxton L J, Zheng Y. 2008. Interplanetary shock induced ring current auroras. J Geophys Res-Space, 113: A01212.

Zhou S, Luan X, Søraas F, et al. 2018. The detached auroras induced by the solar wind pressure enhancement in both hemispheres from imaging and in situ particle observations. J Geophys Res-Space, 123: 3170-3182.

Zhou X, Haerendel G, Moen J I, et al. 2017. Shock aurora: Field-aligned discrete structures moving along the dawnside oval. J Geophys Res-Space, 122: 3145-3162.

Zhou X, Tsurutani B T. 1999. Rapid intensification and propagation of the dayside aurora: Large scale interplanetary pressure pulses (fast shocks). Geophys Res Lett, 26: 1097-10100.

Zhou X, Tsurutani B T. 2001. Interplanetary shock triggering of nightside geomagnetic activity: Substorms, pseudobreakups, and quiescent events. J Geophys Res-Space, 106: 18957-18967.

Zhou X Y, Strangeway R J, Anderson P C, et al. 2003. Shock aurora: FAST and DMSP observations. J Geophys Res-Space, 108(A4): 8019, doi:10.1029/2002JA009701.

Zhou X Y, Fukui K, Carlson H C, et al. 2009. Shock aurora: Ground-based imager observations. J Geophys Res-Space, 114: A12216, doi: 10.1029/2009JA014186.